Cascadability and reshaping properties of a saturable absorber inserted inside a RZ transmission line for future 160-Gbit/s all-optical 2R-regenerators

Julien Fatome, Stéphane Pitois, David Massoubre, Jean-Louis Oudar, Guy Millot

Cascadability and reshaping properties of a saturable absorber inserted inside a RZ transmission line for future 160-Gbit/s all-optical 2R-regenerators

J. Fatome[1], S. Pitois[1], D. Massoubre[2], J-L. Oudar[2] and G. Millot[1]

[1]*Institut Carnot de Bourgogne (ICB), dept OMR, UMR-CNRS 5209, Université de Bourgogne, 9 av. Alain Savary, BP 47870, 21078 Dijon, France*

[2]*Laboratory for Photonic and Nanostructures, UPR-CNRS 20, Route de Nozay, 91460 Marcoussis, France*

Author e-mail address : Julien.Fatome@u-bourgogne.fr

Abstract — In this prospective work, we analyze the behavior of a quantum-well microcavity saturable absorber component cascaded into a 100-km SMF RZ transmission line in order to annihilate the ghost-pulse phenomenon in the following simplified "…010101…" 160-Gbit/s 2-bit pattern at 1555 nm. Recirculating-loop experiments show a maximal ghost-pulse extinction up to 11.6 dB as well as an intensity extinction ratio enhancement higher than 6 dB over at least 800 km of propagation.

I – INTRODUCTION

With the deployment of the first 40 Gbit/s telecommunication systems in the forthcoming years, more and more attention is being paid to transmission lines working at higher bit-rates, such as 160 Gbit/s [1]. However, many studies reveal that these future networks, based on the transmission of picosecond or even sub-picosecond pulses, will suffer from low tolerance against cumulative propagation impairments, such as broadening due to chromatic and polarization mode

dispersions or ghost-pulse generation into the “0” bit-slots due to intra-channel four-wave mixing [2]. Moreover, because of the limit bandwidth of electronic devices, any regeneration or conversion stage at bit rates higher than 80 Gbit/s must be done in the optical domain. Consequently, there is no doubt that all-optical high-speed 2R-regenerators (reamplification and reshaping) will play a preponderant role in increasing the maximum transmission distance of these future ultra-high bit-rate systems [3]. Preliminary experiments of signal reshaping at 160 Gbit/s have already been successfully done in back-to-back configurations by means of Semiconductor Optical Amplifiers (SOA) [4], Nonlinear Optical Loop Mirrors (NOLM) [5] as well as in a recirculating-loop 3R-regenerator experiment based on nonlinear polarization rotation [6]. An alternative approach consists in using Saturable Absorber (SA) devices which are totally passive, polarization independent and easy to use. Transmission experiments have already proved their cascadability and inline efficiency at 10 Gbit/s and 40 Gbit/s [3, 7], and they even may reshape several wavelengths on the same chip [3]. But, although the response time of this kind of component was proved to be fully compatible with future 160-Gbit/s applications [8-9], as far as we know, no inline investigation was yet available in the literature. This is the reason why, in this prospective work, we analyze the cascadability and reshaping properties of a quantum well microcavity Saturable Absorber device cascaded inside a 100-km Single Mode Fiber (SMF)-based RZ transmission line cadenced at 160 GHz. The efficiency of our component is characterized by injecting the simplified and degraded 160-Gbit/s “…010101…” 2-bit pattern into a recirculating-loop setup and by comparing the signal quality through the transmission line with and without the insertion of the regenerative module. The optical autocorrelation function, dramatically sensitive to an Intensity Extinction Ratio (IER) degradation, was used to characterize the signal quality and shows that an improvement of more than 6 dB of the

propagative RZ-data IER can be achieved over at least 800 km when the SA device is inserted into the loop.

II – EXPERIMENTAL SETUP

The experimental setup is schematically represented in Fig. 1. A high quality well-separated pedestal-free 80-GHz 2.4-ps pulse train is generated at 1555 nm by means of the multiple four wave mixing process taking place into 1420 m of Teraligth fiber [10]. Then, in order to test the reshaping efficiency of our SA device for future 160-Gbit/s applications, this 80-GHz pulse train is multiplexed into the time domain to build the following degraded 160-Gbit/s 2-bit pattern "…010101…" in which the energy of the ghost-pulses localized into the "0" bit-slots can be adjusted owing to a variable attenuator (Att). The resulting signal is then injected into a transmission line made of 100 km of SMF fiber followed by a dispersion compensating module (DCF) which fully compensates both the second- and third-order chromatic dispersions. Two Erbium doped fiber amplifiers (EDFA) are used to compensate for the total losses of the line (34 dB without the regenerative module, 44 dB with) while a 1.8-THz optical band pass filter (OBPF) reduces the accumulation of noise into the loop. The regenerative module (dashed-box in Fig. 1) is composed by an EDFA, a circulator and a fiber-pigtailed high aperture lens producing a focus spot of 5 µm diameter (at $1/e^2$) on the SA device. Note that in presence of the regenerative module, the 1.8-THz OBPF also attends to limit the spectral broadening of the transmitted signal thus, stabilizing the SA propagation regime [7]. After propagation through the transmission line, the output signal is finally characterized by a background-free second-harmonic generation autocorrelator.

III – SATURABLE ABSORBER STRUCTURE

The structure of the SA device reported in this paper is schematically represented in Fig. 2a. Its structure and principle of operation are similar to the ones reported elsewhere [7-9, 11]. It consists of an active layer (7 InGaAs/InP quantum wells) comprised inside an asymmetric Fabry-Perot micro-cavity and suitably located at the antinodes of the intracavity intensity. After metal-organic vapour phase epitaxy (MOVPE) growth, the structure underwent 12°MeV Ni^{6+} ion irradiation with a dose of $1x10^{12}$ cm^{-2}. Such energetic ions create clusters of defects along the ion path through the active layer. These defects act as carrier recombination centers, which reduce the carrier lifetime from a few nanoseconds to the picoseconds range [12], thus yielding our component compatible with high bit-rate operations. Pump and probe measurement at 1.55 µm showed a response time of 1 ps while previous published works have already demonstrated that our component is able to reshape not only consecutive “1s” cadenced at 160 GHz [8] but also a sequence made of “0” levels followed or preceded by “1s”, and separated by 6.25 ps [9], proving that our SA component is fully timing-compatible with future 160-Gbit/s regeneration applications. The back mirror was made by the deposition of a thin silver (Ag) layer, then a top-down mounting was made by soldering this Ag film onto a silicon wafer thanks to an In-Au metallic bonding to improve the heat dissipation. A finely controlled chemical etching of the top InP phase layer permitted the resonance matching with the quantum well excitonic absorption wavelength. Finally a two period dielectric layer ($2x\ SiO_2/TiO_2 : \lambda/4 / \lambda/4$) was deposited as front mirror of the cavity. The microcavity resonance has a typical –3 dB bandwidth of 50 nm centered at 1.55 µm and it was designed to have a reflectivity close to zero at low intensity (impedance matching).

IV – EXPERIMENTAL RESULTS

First of all, we have measured the nonlinear power transfer function of our component (Fig. 2b) by determining the ratio of the total energy contained in the ghost-pulses at the output of the SA device as a function of the input ratio. This curve was obtained in a back-to-back configuration at 1561 nm and for a SA input average power of 19 dBm (80mW) owing to the degraded 160-Gbit/s bit-pattern in which the energy contained in the input “0” bit-slots is adjusted by simply tuning the variable attenuator of the source setup represented in Fig. 1 [10]. As expected, our SA device is characterized by a strong nonlinear response with a large discrimination of low powers which is essential for any all-optical regeneration processing.

In a second time, we have optimized our regenerative module by determining the optimum SA input average power providing the maximum intensity extinction ratio (IER) improvement after 100 km of propagation. Figures 3a and 3b show respectively the autocorrelation functions of the 160-Gbit/s 2-bit pattern after 100 km of propagation and the corresponding ratio of total energy contained in the ghost-pulses as a function of the SA input average power. The dashed-curve represents the input degraded signal (Fig. 3a) as well as its initial level of energy in “0” (Fig. 3b). We can clearly see that there exits an optimum input average power, 16 dBm, for which a large improvement of the signal quality is observed. The ratio of energy contained in the ghost-pulses localized in the “0” bit-slots is then reduced from 10.4% at 0 km to only 1.3% after 100 km of propagation in the SA transmission line, which corresponds to a 9 dB improvement of the IER. Note that, after reshaping on the SA device, no dramatic change was noticed on the “1”-bit pulses, except a small temporal compression from 2.4 ps to 2.0 ps. When the average power is increased above 16 dBm, the ghost-pulse extinction decreases significantly due to a thermal shift of the spectral resonance with increasing power [11]. Note that the optimum average power

measured in this section is 3 dBm lower than those reported in the back-to-back configuration experiment thanks to a better management of thermal effects due to a lower working wavelength.

A third series of experiments was carried out in order to study the cascadability and reshaping properties of our SA device during the transmission stage. Figures 4a and 4b represent the autocorrelation functions of the 160-Gbit/s 2-bit pattern as a function of the propagation distance in absence (a) and in presence (b) of the regenerative module. In both cases, the input average power of the line was fixed to 10 dBm while the SA input average power was tuned to the optimum value reported above, i.e. 16 dBm. From Figs. 4, we can clearly observe a large improvement of the signal quality owing to the SA device. Indeed, at each round trip of the loop, the ghost-pulse energy keeps growing in the SA-free configuration (Fig. 4a) whereas in presence of the SA regenerative module (Fig. 4b), the energy remains always much lower than its initial level for the same range of propagation distance. More precisely, from autocorrelation traces, we have calculated the ratio of total energy localized in the ghost-pulses at the output of the loop as a function of the propagation distance. These results are represented in Fig. 5a in absence (circles) and in presence (triangles) of the regenerative module. We can observe that our SA device is strongly efficient to reduce the presence of ghost-pulses, demonstrating clearly its cascadability and regenerative efficiency with an amount of energy contained in the “0” bit-slots always lower than its initial one. At the opposite, in the none-regenerative configuration, we can notice that the energy localized in the “0” bit-slots carries on growing all along the propagation. Fig. 5b completes the analyses by showing in a logarithm scale the evolution of the signal IER as a function of the propagation distance compared to its initial level (input of the line at 0 km). In absence of regenerative module (circles), as the energy contained in the “0” bit-slots increases continuously during the whole transmission stage, the IER improvement remains negative, meaning a constant degradation of the signal. At the opposite, owing to the insertion of the SA

component (triangles), the signal quality is significantly improved all along the 800 km of propagation, reaching a maximum IER enhancement of 11.6 dB at 300 km (0.7 % of energy in "0" vs 10.4 % at 0 km). More roughly, we can notice that all along the 800 km of propagation, the signal IER remains up to 6 dB higher than in the configuration without the SA component, demonstrating the reshaping potential of this kind of component for future 160-Gbit/s regenerators. We would like to emphasize that above 800 km of propagation with the SA component, no measurement could be performed, because of a high instability of the optical signal presumably due to the absence of a level-stabilizing device that would regenerate the "1"-symbols and thus limiting the cascadability potential of our component. In order to clarify this point, by means of the method described in reference [13], we derived from autocorrelation traces the Full Width at Half Maximum (FWHM) as well as timing and amplitude jitters of the 160-Gbit/s transmitted signal until 600 km of propagation. Results are presented in Figs. 6. In Fig. 6a, we can observe the evolution of the pulse width as a function of propagation distance. While the FWHM gradually increases all along the propagation in the line without SA component, it slightly decreases and stabilizes by means of the insertion of the regenerative module coupled with the OBPF, proving the cascadability and the efficiency of our component to combat the cumulative broadening impairments due to chromatic and polarization mode dispersions. Fig. 6b and 6c represent the timing and amplitude jitters as a function of propagation distance. We can notice in Fig. 6b that timing jitters follow roughly the same behavior in both configurations stressing that no improvement and even a small degradation is occurred with the insertion of the component. The main difference can be stressed owing to the evolution of the amplitude jitter, represented on Fig. 6c. We can clearly see that the presence of the component dramatically increases the amplitude jitter of the transmitted signal compared to the configuration without SA. This behavior is in agreement with the nonlinear response of this kind of component which

amplifies the peak-power variations at each round trip. This phenomenon underlines the limit of the cascadability of our component and that this SA device is able to correctly regenerate the “0” bit-slots but needs a second stage of regeneration to stabilize the “1” levels such as, a semiconductor optical amplifier [4], or by soliton technique [3]. Note that this high level of amplitude jitter could explain the growing instability of the optical signal observed during the propagation, confirming the necessity of a “1”-symbols level-stabilizing device and raises the idea that in order to achieve the maximum transmission distance, additional studies should be required to determine the optimum regenerative path which does not necessarily correspond to the amplification span [7, 14] as well as the impact of the dispersion map [14].

V – CONCLUSION

In this work, we have studied the cascadability and inline reshaping properties of an all-optical gate based on a passive saturable absorber microcavity. A signal extinction ratio improvement higher than 6 dB was demonstrated over at least 800 km by studying the propagation of a degraded 160-Gbit/s “...010101…” 2-bit sequence into a 100-km SMF/DCF fiber link recirculating-loop setup. Our observations, based on autocorrelation function measurements, clearly indicate that the inline insertion of the saturable absorber device can strongly combat the transmission cumulative impairments such as ghost-pulses and broadening due to intra-channel four-wave mixing, chromatic or polarization mode dispersions. We have also pointed out the main drawback inherent to this kind of component, which is a dramatic increase of the transmitted signal amplitude jitter but which should be reduced by means of a “1”-symbols level-stabilizing device. Finally, although these prospective results have to be confirmed owing to a 160-Gbit/s pseudo-random bit-sequence experiment, we believe that this kind of component,

which adds passivity, low-cost fabrication, experimental setup simplicity and efficient “0” reshaping, appears as a promising candidate for low-cost all optical and passive 2R-regeneration at 160 Gbit/s.

VI – ACKNOWLEDGEMENT

This work is supported by the « Agence Nationale pour la Recherche », Télécommunications 2006, project « FUTUR », 06 TCOM 016.

VI – REFERENCES

1. S. Weisser, S. Ferber, L. Raddatz, R. Ludwig, A. Benz, C. Boerner and H. G. Weber, “Single- and Alternating Polarization 170-Gbit/s Transmission up to 4000 km using Dispersion-Managed Fiber and all-Raman Amplification”, IEEE Photon. Technol. Lett, **18**, 1320-1322 (2006).

2. R.-J. Essiambre, B. Mikkelsen and G. Raybon, “Intra-channel cross-phase modulation and four-wave mixing in high-speed TDM systems”, Electron. Lett., **35**, 1576-1578 (1999).

3. D. Rouvillain, F. Seguineau, L. Pierre, P. Brindel, H. Choumane, G. Aubin, J.-L. Oudar, and O. Leclerc, “Optical 2R regenerator based on passive saturable absorber at 40 Gbit/s for WDM long haul transmissions”, Electron. Lett., **38**, 1113-1114 (2002).

4. J. Leuthold, L. Möller, J. Jaques, S. Cabot, L. Zhang, P. Bernasconi, M. Cappuzzo, L. Gomez, E. askowski, E. Chen, A. Wong-Foy and A. Griffin, “160 Gbit/s SOA all-optical wavelength converter and assessment of its regenerative properties”, Electron. Lett., **40**, 554-555 (2004).

5. A. Bogoni, P. Ghelfi, M. Scaffardi and L. Poti, “All-Optical Regeneration and Demultiplexing for 160-Gb/s Transmission Systems using NOLM-Based Three-Stage Scheme”, IEEE J. Select. Topics Quant. Electron., **10**, 192-195 (2004).

6. S. Watanabe, F. Futami, R. Okabe, Y. Takita, S. Ferber, R. Ludwig, C. Schubert, C. Schmidt and H. G. Weber, “160 Gbit/s Optical 3R-Regenerator in a Fiber Transmission Experiment”, in *Optical Fiber Communication (OFC’03)*, Atlanta, GA, Post deadline paper PD16 (2003).

7. M. Gay, L. Bramerie, D. Massoubre, A. O’Hare, A. Shen, J. L. Oudar, and J. C. Simon, “Cascadability Assessment of a 2R Regenerator Based on a Saturable Absorber and a Semiconductor Optical Amplifier in a Path Switchable Recirculating Loop”, IEEE Photon. Technol. Lett., **18**, 1273-1275 (2006).

8. D. Massoubre, J.-L. Oudar, J. Fatome, S. Pitois, G. Millot, J. Decobert and J. Landreau, “All-optical extinction ratio enhancement of a 160 GHz pulse train using a saturable absorber vertical microcavity”, Opt. Lett., **31**, 537-539 (2006).

9. J. Fatome, S. Pitois, A. Kamagate, D. Massoubre, J-L. Oudar, and G. Millot, “All-optical reshaping based on a passive saturable absorber microcavity device for future 160-Gbit/s applications”, IEEE Photon. Technol. Lett., **19**, 245-247 (2007).

10. J. Fatome, S. Pitois and G. Millot, “20-GHz to 1-THz repetition rate pulse sources based on multiple four wave mixing in optical fibers”, IEEE J. Quant. Electron., **42**, 1038-1046 (2006).

11. D. Massoubre, J.-L. Oudar, A. O'Hare, M. Gay, L. Bramerie, J.-C. Simon, A. Shen, and J. Decobert, "Analysis of Thermal Limitations in High-Speed Microcavity Saturable Absorber All-Optical Switching gates", J. Lightw. Technol., **24**, 3400-3408 (2006).

12. I. Joulaud, J. Mangeney, J.-M. Lourtioz and P. Crozat, "Thermal stability of ion-irradiated InGaAs with (sub-) picosecond carrier lifetime" Appl. Phys. Lett., **82**, 856-858 (2003).

13. J. Fatome, J. Garnier, S. Pitois and G. Millot, "All-Optical Measurement of Background, Amplitude and Timing Jitter for high speed pulse trains or prbs sequences using autocorrelation function", *in Proceedings of European Conference on Optical Communication (ECOC'06)*, Cannes, France, paper We3.P.43 (2006).

14. S. Waiyapot, S. K. Turitsyn, M. P. Fedoruk, A. Rousset and O. Leclerc, "Optical 2R regeneration at 40 Gbit/s using saturable absorber in long-haul dispersion-managed fiber links", Opt. Commun., **232**, 145-149 (2004).

Figure Captions

Fig. 1. Experimental setup, (OS: Optical Switch).

Fig. 2. (a) Saturable Absorber structure. **(b)** Ratio of the total energy contained in the ghost-pulses at the output of the SA device as a function of the input ratio in a back-to-back measurement configuration.

Fig. 3. (a) Autocorrelation functions of the 160-Gbit/s bit-pattern as a function of the SA input average power after 100 km of propagation; the dashed-line shows the initial degraded 160-Gbit/s signal. **(b)** Corresponding ghost-pulse extinction as well as ratio of total energy contained in the ghost-pulses (the dashed-line/circles corresponds to the initial level).

Fig. 4. Autocorrelation functions of the 160-Gbit/s 2-bit pattern as a function of the propagation distance **(a)** In absence of the SA regenerative module, from bottom to top: at 0 km (dashed-curve), 300, 500 and 800 km. **(b)** In presence of the SA device, from bottom to top: at 300, 500, 800 and 0 km (dashed-curve).

Fig. 5. (a) Ratio of the total energy contained in the “0” bit-slots as a function of propagation distance: without SA (circles) and with SA (triangles). **(b)** IER evolution in dB compared to its initial level (0 km) as a function of the propagation distance: without SA (circles) and with SA (triangles).

Fig. 6. (a) FWHM as a function of propagation distance: without SA (circles) and with SA (triangles). **(b)** Timing jitter as a function of propagation distance **(c)** Amplitude jitter as a function of propagation distance.

J. Fatome *et al.* Fig. 1.

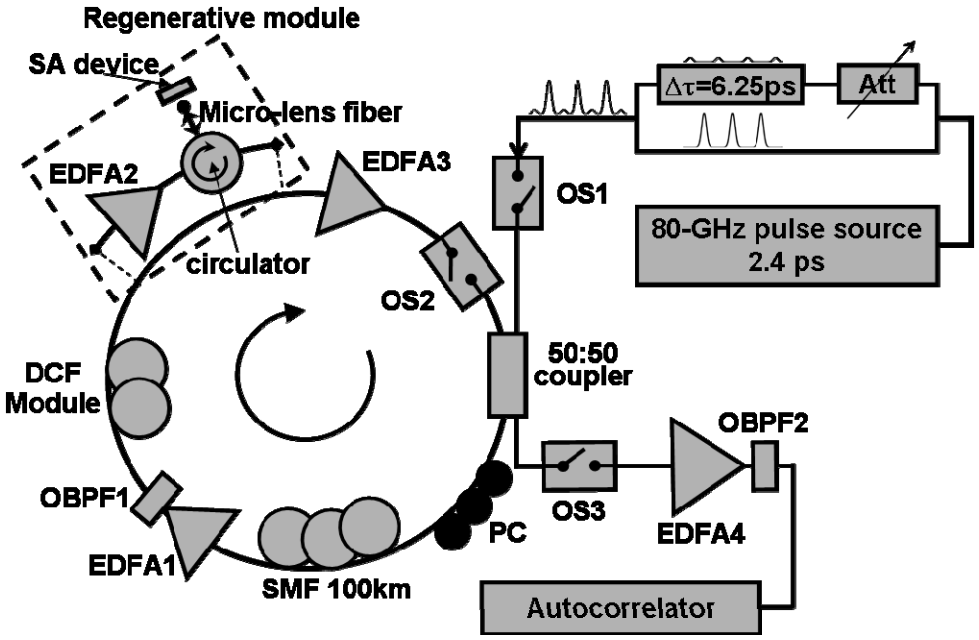

Fig. 1. Experimental setup, (OS: Optical Switch).

J. Fatome *et al.* Fig. 2.

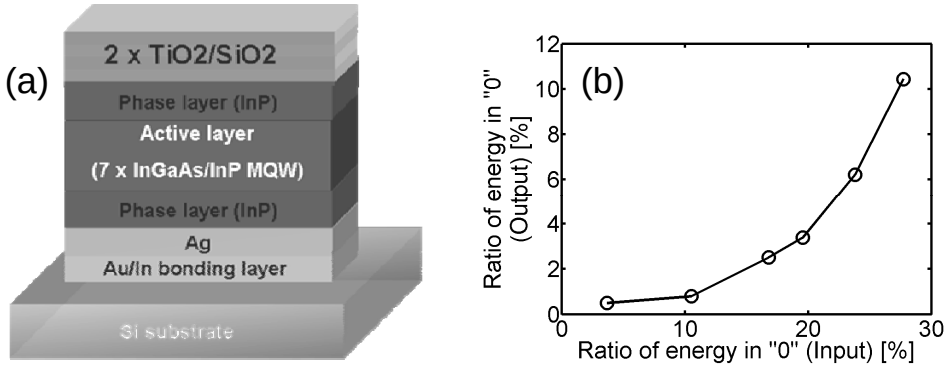

Fig. 2. (a) Saturable Absorber structure. **(b)** Ratio of the total energy contained in the ghost-pulses at the output of the SA device as a function of the input ratio in a back-to-back measurement configuration.

J. Fatome *et al.* Fig. 3.

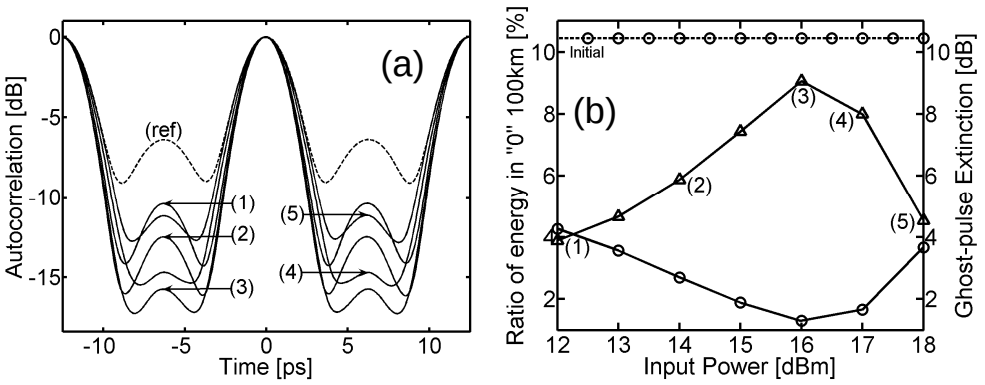

Fig. 3. (a) Autocorrelation functions of the 160-Gbit/s bit-pattern as a function of the SA input average power after 100 km of propagation; the dashed-line shows the initial degraded 160-Gbit/s signal. **(b)** Corresponding ghost-pulse extinction (dB) as well as ratio of the total energy contained in the ghost-pulses (the dashed-line/circles corresponds to the initial level).

J. Fatome *et al.* Fig. 4.

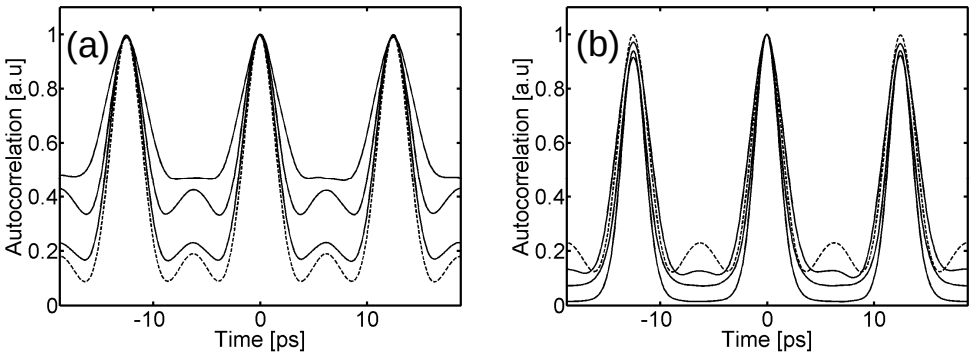

Fig. 4. Autocorrelation functions of the 160-Gbit/s 2-bit pattern as a function of the propagation distance **(a)** In absence of the SA regenerative module, from bottom to top: at 0 km (dashed-curve), 300, 500 and 800 km. **(b)** In presence of the SA device, from bottom to top: at 300, 500, 800 and 0 km (dashed-curve).

J. Fatome *et al.* Fig. 5.

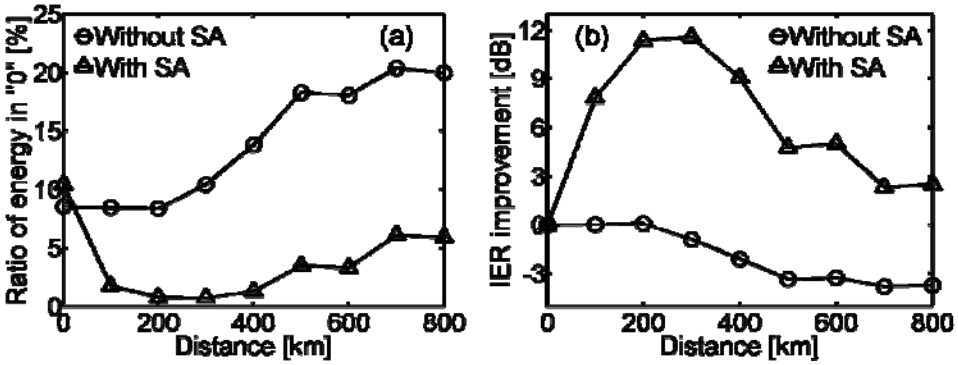

Fig. 5. (a) Ratio of the total energy contained in the "0" bit-slots as a function of propagation distance: without SA (circles) and with SA (triangles). **(b)** IER evolution in dB compared to its initial level (0 km) as a function of the propagation distance: without SA (circles) and with SA (triangles).

J. Fatome *et al.* Fig. 6.

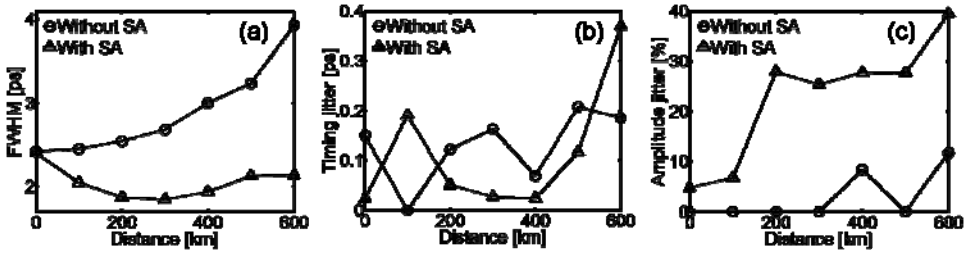

Fig. 6. (a) FWHM as a function of propagation distance: without SA (circles) and with SA (triangles). **(b)** Timing jitter as a function of propagation distance **(c)** Amplitude jitter as a function of propagation distance.